Quantifying Tool Path Deviations in Robotic Continuous Ultrasonic Welding of Thermoplastic Composites

S.H. Han, J.M. van Stuyvesant Meijen, B.C.P. Jongbloed
SAM XL
TU Delft Campus
Rotterdamseweg 382c
Delft 2629HG NL

ABSTRACT

This study investigates the positional accuracy and deformation behaviour of a robotic system performing simulated Continuous Ultrasonic Welding of thermoplastic composites. Thermoplastic composites are attractive due to their high specific properties and can be processed with lower-cost and faster assembly methods. Using a custom-developed end effector on a KUKA KR560 robot, a series of welding motion tests were conducted to analyse lateral deviation and tilt errors during CUW, without activating ultrasonic vibrations. High forces involved in the process result in consistent horizontal slip and tilt at motion initiation, attributed to static friction and stored mechanical energy in the system. Measurements from a laser tracker, force/torque sensors, and triangulation sensors revealed that robot pose and weld-line distance significantly influence these deflections. Notably, deflections were consistent and repeatable, suggesting potential for compensation via calibration or feedback control. Additionally, internal deformation within the end-effector structure and Force Torque sensor assembly contributed to the observed positioning errors. Recommendations include improving frame symmetry and stiffness to reduce mechanical distortion. These findings aim to support more accurate and reliable Continuous Ultrasonic Welding implementation in aerospace-grade composite manufacturing.

1. INTRODUCTION

Thermoplastic composites are attractive materials due to their high strength and stiffness despite being lightweight. The thermoplastic matrix used allows for reshaping or fusion bonding, which may offer lower-cost production and faster assembly methods that are attractive to industries where these may be crucial, such as aerospace manufacturing.

Ultrasonic welding is a method of fusion bonding thermoplastic composites together. Two adherends are placed in overlap, and a sonotrode is placed on them. The sonotrode applies a static welding force while applying ultrasonic mechanical vibrations. The vibrations cause cyclic compression of the to-be-welded components, generating heat through the internal and surface friction which melts and fuses the thermoplastic parts together. The heat generation is focussed at the interface between the two adherends by placing an energy director (ED) between them. The ED is additional resin in the form of ridges, thin film, or mesh[1, 2]; the purpose of which is to create increased compliance and additional surface contact to generate more heat. By moving the sonotrode as the material melts, it is possible to continuously weld material, which is called continuous ultrasonic welding (CUW)[3, 4]. To prevent the just-welded material from de-consolidating, a consolidator precedes the sonotrode, which cools and applies pressure[5].

Industrial robots, which are used as manipulators for CUW, are not perfectly accurate nor stiff and deflect under loads. The end-effector applies a force of approx 5000 N which is a significant load on an industrial robot and can cause deflections. Understanding these deflections is paramount because the CUW process is sensitive to misalignment of the sonotrode. Misalignment can not only result in welding the adherends at a misaligned angle, but it can also affect the heat generation, affecting the quality of the weld[6].

Therefore, this paper will study the positional accuracy of a robot during CUW, with a focus on tracking the horizontal positioning error and side tilt error, which would respectively place the weld in an incorrect location and cause uneven contact of the sonotrode with the adherends, affecting weld quality. This paper investigates the influence of robotic deflection on weld quality in CUW, focusing on horizontal position and tilt errors of the end effector.

2. RESEARCH TESTS & EXPERIMENTS

This section describes the equipment and procedure used to obtain the results shown in .

2.1. Experimental Setup

Welding motions were executed with an in-house developed CUW end effector (EEF) on a Vansichen track-mounted KUKA KR560 R3100-2 robot arm, shown in Figure 1 and Figure 4. The robot is connected to the EEF through a quick coupler with a Force Torque (FT) sensor, which is 17 degrees off-axis of the tool center point (TCP). The TCP is the sonotrode tip; the EEF also has a compactor and consolidator which precede and trail the sonotrode respectively. A rounded sonotrode tip is used which makes tilting forward/rearward of the sonotrode less critical [7]. The sonotrode is mounted to the rear plate through a carriage of linear rails that allows for vertical deployment of the sonotrode assembly. The distance between the sonotrode center and the rear plate is 110 mm. A cross-sectional diagram of this assembly is shown in Figure 2.

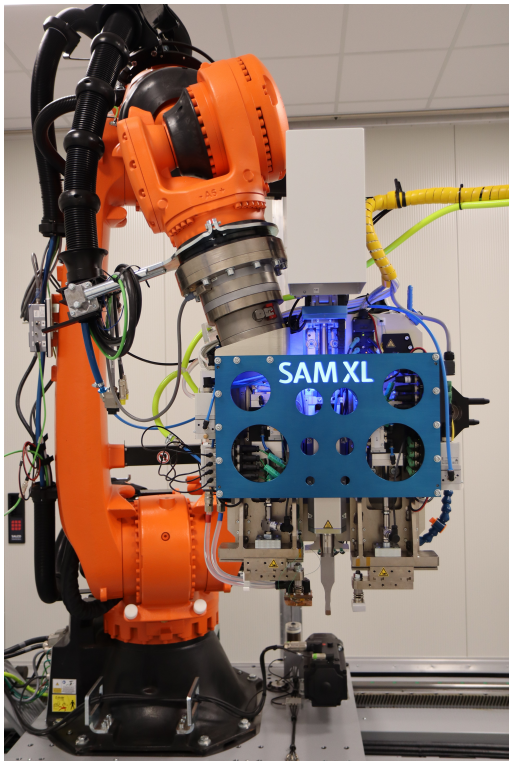

Figure 1: Front view of SAM XL Continuous Ultrasonic Welding end effector on KUKA KR560 R3100-2 robot

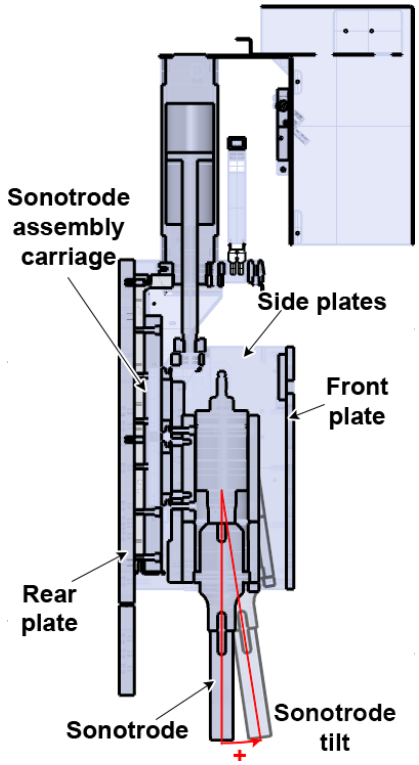

Figure 2: Cross-section of EEF seen from the side with sonotrode mounting.

An overview of sensors used in this study is given in Table 1. A Leica TMAC mounted on the welding direction side, 333.2 mm above the TCP, is tracked by a Leica AT960 absolute laser tracker (AT) to measure the pose of the EEF. The TMAC measured position is transformed to the TCP location to track the TCP. KUKA Robot Sensor Interface (RSI) software package

extracts data from the robot controller. A ScanCONTROL 3010-100 laser line triangulator (LLT) views the sonotrode-adherend contact area at an angle, as shown in Figure 3, measuring the angular deflection of the sonotrode. The FT sensor measures the forces and torques transferred through the EEF to the robot flange.

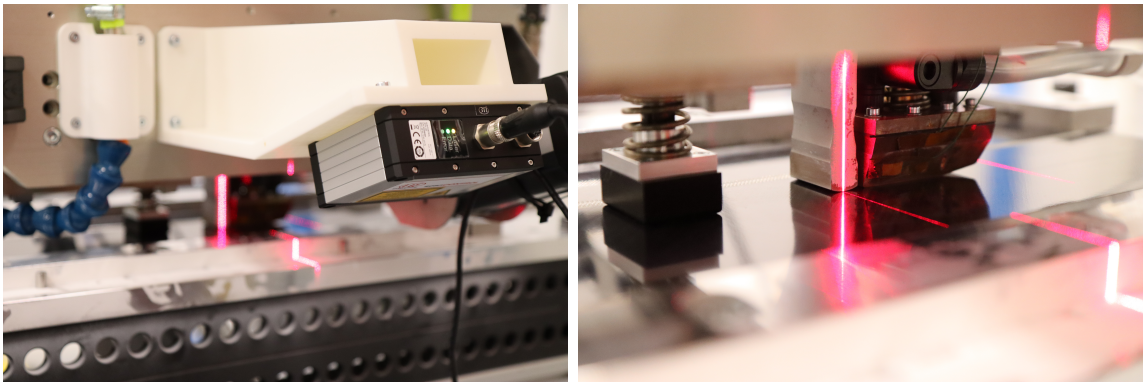

(a) LLT mounted to EEF frame

(b) Laser line on sonotrode, top adherend and jig wall

Figure 3: Laser Line Triangulator (LLT) pointed at sonotrode contact region

Table 1: Overview of sensors used with their data description

Equipment	Acronym	Data collected	Rate
KUKA Robot Sensor Interface	RSI	TCP Cartesian position X, Y, Z (mm) TCP Euler angle Rx, Ry, Rz (°) Joint angles $A1$, $A2$, $A3$, $A4$, $A5$, $A6$ (°)	250 Hz
Leica AT960-MR w/ T-MAC	AT	TCP Cartesian position X, Y, Z (mm) TCP Euler angle Rx, Ry, Rz (°)	250 Hz
Micro-Epsilon LLT3010-100	LLT	Sonotrode angle θ_{TCP} (°)	50 Hz
SCHUNK FTN-OMEGA191	FT	Forces Fx, Fy, Fz (N) Moments Tx, Ty, Tz (Nm)	30 Hz

2.1.1. Welding jig and material used

Unidirectional carbon-fibre reinforced PPS adherends ($[45/0/135/0/0/90/0]_S$ layup, 2.14 mm thick) with PPS woven mesh (0.47 mm thick, 53% open area) energy director in between the adherends were used. The plates were placed inside a picture frame jig in an overlapping configuration constraining in-plane movement.

2.2. Experiments

Several experiments with welding motions were conducted without having the ultrasonic vibrations on. An overview of the experiments is given in Table 2 and corresponding illustrations shown in Figure 4. All tests were carried out with 2200 N consolidator force, 1800 N sonotrode force and 1000 N compactor force.

2.2.1. TCP accuracy during welding

To investigate the accuracy of TCP movement during welding motions the EEF was tracked by AT as it moved in several configurations. In config. 1 the robot moves the EEF parallel to

its linear track along a line 1300 mm distance from its base (red arrow labelled 1 in Figure 4a). In 1t, while the TCP moves along the same line, the linear track also moves the base of the robot (blue arrow labelled t) which results in the robot almost not moving. Config 2 and 2t are the same as 1a and 1t, respectively, but with the weld line positioned farther away from the robot, 2200 mm away. Configuration 3 differs in that instead of parallel, the robot pushes the EEF perpendicular away from itself in the direction marked with a red arrow and labelled 3 in Figure 4b.

Table 2: Test configurations jig position

Configuration	Distance from robot	Movement by	TCP angle R_x
1	1300 mm	Robot parallel	0°
1t	1300 mm	Linear track	0°
2	2200 mm	Robot parallel	0°
2t	2200 mm	Linear track	0°
3	1300 to 2200 mm	Robot perpendicular	0°

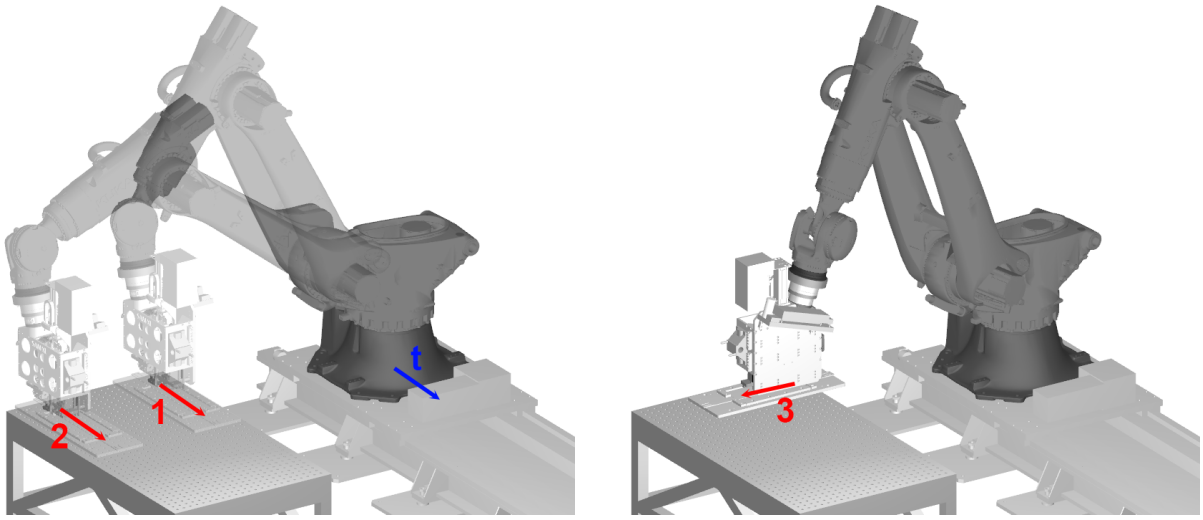

(a) Parallel motion configurations (b) Perpendicular motion configurations

Figure 4: Schematic of various welding motion configurations

2.2.2. Effect of contact angle on end effector and sonotrode deflection

To investigate the effect of contact angle on the sonotrode deflection, configuration 1 tests were repeated with intentional rotation around welding direction, *Rx*, (+0.5°, +0.2°, -0.2°, -0.5°). AT measured the EEF side slip and side tilt, while the LLT measured the sonotrode tilt as the welding motions occurred at various contact angles.

2.2.3. Deflection measurement of FT sensor assembly

The FT sensor region was measured with a Zeiss ATOS metrology scanner (sensor, region and reference stickers shown in Figure 5) for deformations in the FT sensor. Three states were measured; actuators undeployed, deployed with force and after moving with the actuators

deployed. The deviation of the deployed state and after-move state from the undeployed state are later referred to 'Deployed' and 'Movement' respectively.

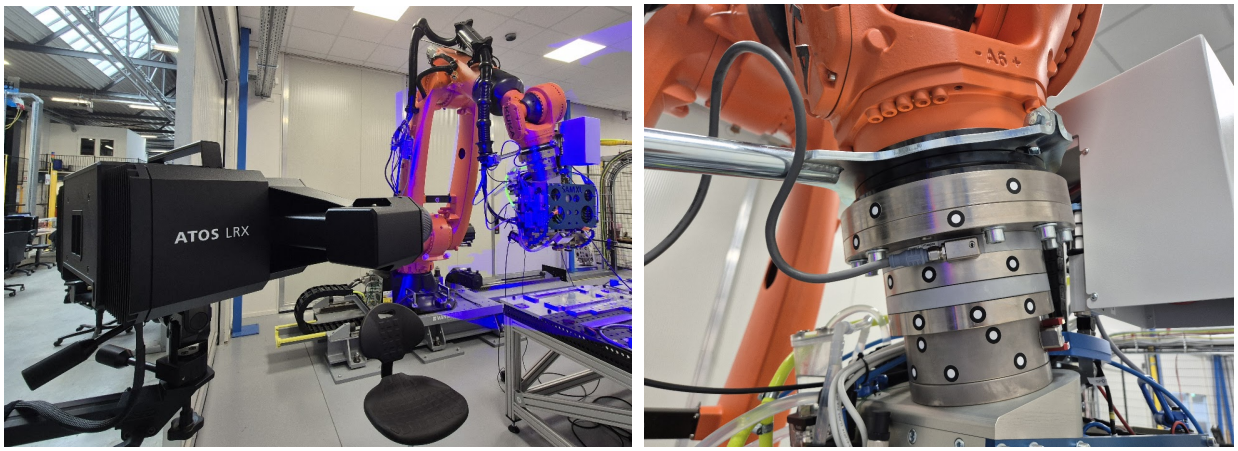

(a) Zeiss ATOS LRX measuring robot and end-effector

(b) Reference point stickers applied to coupling area

Figure 5: Deformation measurement of Force Torque sensor

3. RESULTS

This section presents the results obtained from the tests described in Section 2.

3.1. TCP accuracy during welding

Figure 6a and Figure 6b, respectively show the EEF side slip, Y position, and EEF tilt, Rx rotation, measured by the laser tracker for a full weld motion for configuration 1a. The first 50 mm of the motion are shown magnified in Figure 7. Figure 7c additionally shows the torque about X captured by the FT sensor.

The mean average value and standard deviation from mean of the smooth region where $50 < X < 200$ mm for the different configurations described in Section 2.2 are given in Table 3 and visualized in Figure 8.

Table 3: Mean average and standard deviation of Y and Rx within stable region (50<X<200 mm)

Test	$\overline{Y}$ (mm)	σY (mm)	$\overline{R_x}$ (°)	σR_x (°)
1a (close robot)	-1.66	0.071	-0.14	0.0052
1t (close track)	-1.89	0.035	-0.16	0.0053
2 (far robot)	-1.94	0.065	-0.18	0.0038
2t (far track)	-1.80	0.048	-0.18	0.0042
3 (push)	-0.86	0.023	-0.046	0.0020

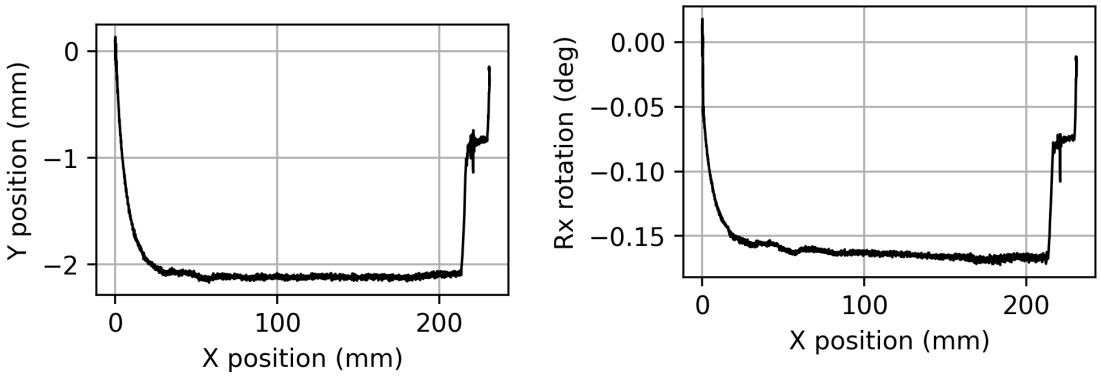

(a) Side slip in Y position

(b) Side tilt around X

Figure 6: Laser tracker measured TCP position over welding motion 1a

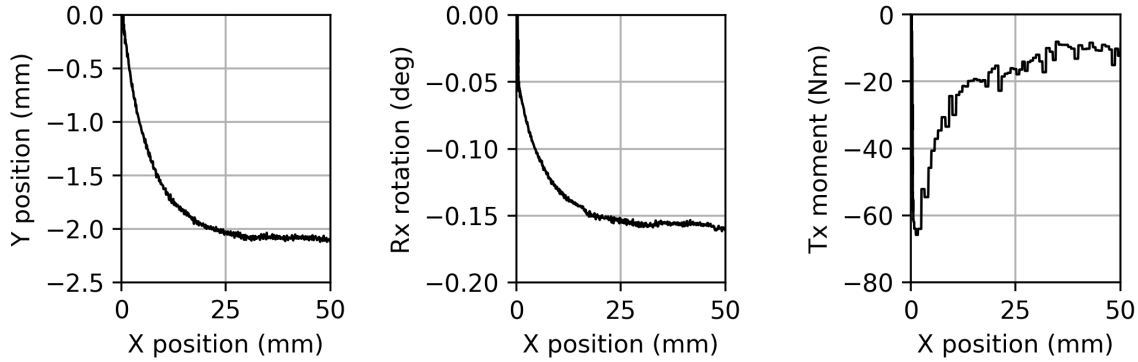

(a) Laser tracker measured sideslip of TCP during weld motion

(b) Laser tracker measured rotation/tilt of TCP during weld motion

(c) Force torque sensor measured moment around welding direction

Figure 7: Slippage behaviour on motion initiation

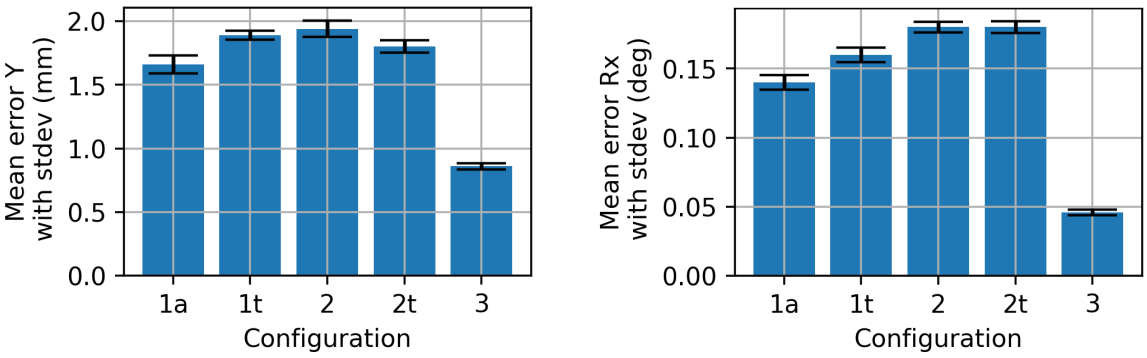

(a) Y side slip error

(b) Rx side tilt error

Figure 8: Average and standard deviation error in different configurations

3.2. Effect of contact angle on end effector and sonotrode deflection

The side-slipping effect under different contact angles are shown in Figure 9. Figure 9a shows the side-tilt showing the same shape previously seen in Figure 7b, with the addition of an angle offset due to the intentional overall tilt programmed into each test. Figure 9b shows the same curves as Figure 9a with their programmed tilts subtracted from the overall values.

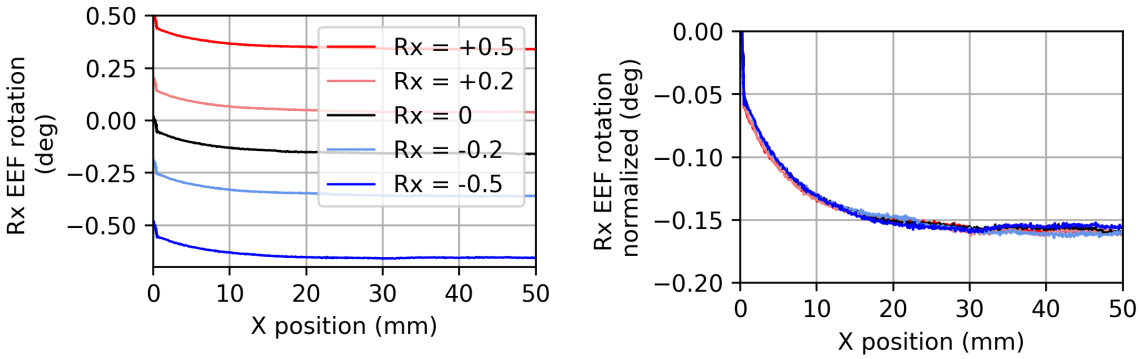

(a) Rotation/tilt response to programmed artificial tilt *Rx*

(b) Same as (a) but with setpoint angle subtract from data

Figure 9: Tilt rotation around X at different artificially programmed tilt angles

Figure 10 shows LLT-measured deflections of the sonotrode during tilted welding motions. In all tests, the sonotrode tilted in the same direction regardless of contact angle tilt direction.

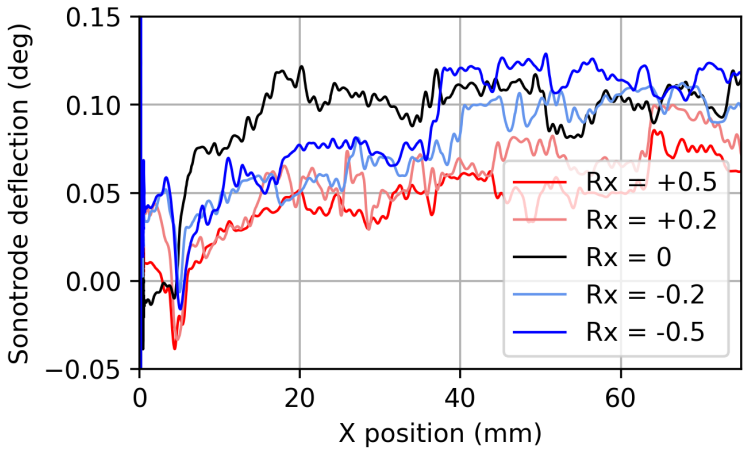

Figure 10: Sonotrode deflection at various programmed EEF tilt measured by LLT

3.3. Deflection measurement of FT sensor assembly

The deflections measured by the Zeiss metrology scanner of the FT sensor assembly are given in Table 4. The values show larger deflections in the 'Deployed' state than in the 'Movement' state, the definitions of which are given in Section 2.2.3.

Table 4: Deflections in Z and rotations around X and Y measured within the coupling region

	ΔZ	ΔR_X	ΔR_Y
Deployed	0.18 mm	-0.10°	-0.08°
Movement	0.12 mm	-0.06°	-0.02°

4. DISCUSSION

Due to the high forces required for the CUW process, various deflections have been observed. Several tests were conducted to explore these deflections, the results shown in Section 3 are discussed in this section.

4.1. TCP accuracy during welding

When the welding motion begins and the TCP starts moving, a sideways slip of approx. 2 mm and rotation of 0.15° is seen in Figure 7 and was also visually observed. Figure 6 shows that after this slipping behaviour, the EEF remains stable throughout the weld until it shifts back toward 0 in two steps as first the sonotrode and compactor, followed by the consolidator, are retracted and no longer apply force. It should be noted that the shift in Y is a sum of pure lateral shift of the whole EEF as well as TCP shift due to the rotation R_x as in Equation 1 (0.15° rotation contributes 0.87 mm to Y shift).

$$\delta Y_{total} = \delta Y_{pure} + 333.2 \cdot tan(\delta R_x) \tag{1}$$

The slipping effect does not happen immediately when forces are applied. The deflections only appear after movement in X direction as can be seen in Figure 7a and Figure 7b. In Figure 7c approx. 60 Nm of torque is registered by the FT sensor which reduces to approx 1 Nm once the motion is underway. Our explanation for this is that the process forces from the EEF create a bending moment on the robot. However, due to friction caused by the high forces at the contact point, the EEF is unable to rotate and is kept in place. Only upon welding motion movement is the static friction overcome and the TCP shifts, and the stored torque about X direction is relieved.

Overall the perpendicular deviations from the welding motion and the rotation around the TCP in welding direction are highly consistent as shown by the standard deviations of the error in Table 3, with standard deviation under 0.2 mm and 0.01° in all configurations. The high consistency of the error allows for it to be removed by calibration to pre-compensate for the slip and tilt. It would be valuable to predict the value of these errors at different robot poses and process forces, so that a correction can be pre-programmed to anticipate and therefore remove this positioning error. The smooth nature of this error also likely makes it possible to correct with sensor-based feedback control.

From Table 3 it was found that having the weld line closer to the robot root has advantages (config. 1 vs 2) in minimizing deflection errors, this effect is most likely caused by the

reduction in distance between the weld-line and robot reducing the moment arm of the forces being applied at the T.

Welding motion with solely the track did not give significantly improved results (configuration 1t and 2t in Table 3). This is believed to be because the robot controller is still active during 'track-only' movements, and must still make minor adjustments to keep the TCP at the programmed position. True track-only movement would only be possible if the welding jig and track were perfectly parallel, which in reality will never be the case.

Figure 8 shows that config. 3 showed lower side slip and rotation deflection compared to config. 1 and 2. This is because the EEF weld direction is co-incident with the base of the the robot, the TCP force moment arm which causes the robot to deflect around X direction becomes near zero.

However, deflections were not completely eliminated and still approximately half of the side slip and a third of the side tilt errors of config. 1 were observed. This result is unexpected and unexplained. One possibility is that this deflection which exists even though the robot pose should eliminate it is caused by the EEF frame itself. The EEF frame is not symmetrical and may be twisting under load and displacing the TMAC from the rest position. More investigation is needed to confirm this, and if this is indeed a cause for deflection, stiffer and/or symmetrical EEF frame designs could be a solution to eliminate it.

4.2. Effect of contact angle on end effector and sonotrode deflection

The results of the contact angle test shown in Figure 9 showed that the EEF always tilts toward the same direction regardless of the contact angle. Figure 9b shows a remarkably consistent tilting behaviour regardless of contact angle. It also shows that there is not enough flexibility in the sonotrode assembly to automatically re-align itself perpendicular to the contacting surface. In retrospect, this is logical, as the moment caused by the moment arm of the entire robot length dwarfs the moment caused by the sonotrode tip being tilted one way or the other.

Similarly to the effects seen in Section 3.2, Figure 10 shows the sonotrode also always tilts towards the same direction regardless of the contact angle. Though smaller in scale, the sonotrode is also mounted in a cantilever fashion, so it shows the same tilting behaviour as the robot when loaded in vertical force. In every test, Figure 10 showed an increase in sonotrode tilt within the first 20 mm of motion; this is probably related to the slipping effect discussed in Section 4.1. The sonotrode tip is locked in place due to friction during force initiation, and deflection only occurs once movement initiates.

The tilt is believed to be caused by play in the carriage system (shown in Figure 2) as well as mechanical deformation caused by the moment of the vertical forces bending the assembly. This too requires further study and possibly could be eliminated by stiffer and symmetrical carriages.

4.3. Deflection measurement of FT sensor assembly

Table 4 shows that when the actuators are deployed with force, the FT sensor area above the EEF tilts by Rx= -0.1°. This condition is equivalent to where X= 0 mm on Figure 7b where Rx is also approx. 0. It is believed that the TCP is unable to tilt but is held in place due to friction at the sonotrode/adherent contact point. Instead, the energy is stored in the form of bending of the EEF frame, FT sensor, and robot links. This -0.1° tilt within the FT sensor is believed to be part of this stored bending. Once the EEF moves and some of this energy is released, the deformation within the FT sensor reduces to -0.06° and manifests externally as a tilt in the TCP's Rx.

5. CONCLUSIONS

A study was conducted on the positional accuracy of a robot performing simulated continuous ultrasonic welding motions. Sensors were used to measure horizontal side shifting, side tilt of the end effector, and side tilt of the sonotrode.

A consistent positioning error was identified, characterized by slipping and tilting of the end effector in a predictable manner. This slipping behaviour appears to depend primarily on the robot's pose and its distance from the base and is not significantly influenced by the sonotrode/adherend contact angle. It is likely also affected by process forces, although this requires further investigation.

Evidence suggests that deformation occurs within the end effector, likely due to frame twisting and tilting of the sonotrode mount. These deformations appear to be repeatable, which suggests they could potentially be compensated for through calibration or control strategies. Designing end effectors with sufficient stiffness—and preferably with symmetrical geometry—can help mitigate such effects. Symmetry is especially important to prevent sonotrode tilt about the welding direction, which is critical for maintaining weld quality in continuous ultrasonic welding.

To accurately track and compensate for deflections, it is essential to use a stiff robot and incorporate external measurements. Otherwise, deflections unknown to the robot controller could go undetected. Additionally, employing a rounded sonotrode tip reduces the demands on robot accuracy, as orthogonality is required in only one direction instead of two. Following the initial slipping behaviour, the end effector exhibited steady motion with low variance, which is promising for the development of sensor-based, closed-loop correction approaches to enhance robotic accuracy in continuous ultrasonic welding.

6. ACKNOWLEDGEMENTS

This work was funded by the Dutch Governnment's National Growth Fund programme under the project NXTGEN Hightech Composites 02: Digital micro-factory for lightweight e-mobility.

7. REFERENCES

[1] I. F. Villegas. "Ultrasonic Welding of Thermoplastic Composites". In: Frontiers in Materials Vol. 6 (2019), p. 291. ISSN: 2296-8016. DOI: 10.3389/fmats.2019.00291. URL: https://www.frontiersin.org/article/10.3389/fmats.2019.00291.

[2] B. Jongbloed, J. Teuwen, G. Palardy, I. F. Villegas, and R. Benedictus. "Continuous ultrasonic welding of thermoplastic composites: Enhancing the weld uniformity by changing the energy director". In: Journal of Composite Materials Vol. 54.No. 15 (2020), pp. 2023–2035. DOI: 10.1177/0021998319890405. eprint: https://doi.org/10.1177/0021998319890405. URL: https://doi.org/10.1177/0021998319890405.

[3] F. Senders, M. van Beurden, G. Palardy, and I. Villegas. "Zero-flow: A novel approach to continuous ultrasonic welding of CF/PPS thermoplastic composite plates". In: Advanced Manufacturing: Polymer & Composites Science Vol. 0340.No. September 2017 (2016), pp. 1–10. ISSN: 2055-0340. DOI: 10.1080/20550340.2016.1253968.

[4] B. Jongbloed, J. Teuwen, R. Benedictus, and I. F. Villegas. "On differences and similarities between static and continuous ultrasonic welding of thermoplastic composites". In: Composites Part B: Engineering Vol. 203 (2020), p. 108466. ISSN: 1359-8368. DOI: https://doi.org/10.1016/j.compositesb.2020.108466. URL: https://www.sciencedirect.com/science/article/pii/S1359836820335149.

[5] B. Jongbloed, R. Vinod, J. Teuwen, R. Benedictus, and I. F. Villegas. "Improving the quality of continuous ultrasonically welded thermoplastic composite joints by adding a consolidator to the welding setup". In: Composites Part A: Applied Science and Manufacturing Vol. 155 (2022), p. 106808. ISSN: 1359-835X. DOI: https://doi.org/10.1016/j.compositesa.2022.106808. URL: https://www.sciencedirect.com/science/article/pii/S1359835X22000057.

[6] M. Ahanpanjeh, F. Köhler, V. Adomat, C. Kober, M. Fette, and J. Wulfsberg. "Impact of Alignment of the Sonotrode on the Quality of Thermoplastic Composite Joints in Continuous Ultrasonic Welding". In: Nov. 2022.

[7] B. Jongbloed, J. Teuwen, and I. F. Villegas. "On the use of a rounded sonotrode for the welding of thermoplastic composites". In: Journal of Advanced Joining Processes Vol. 7 (2023), p. 100144. ISSN: 2666-3309. DOI: https://doi.org/10.1016/j.jajp.2023.100144. URL: https://www.sciencedirect.com/science/article/pii/S2666330923000067.